WAVE CLIMATE CONTROL OF EMBAYED BEACH EQUILIBRIUM BATHYMETRY

Christopher J. Daly[1,2], Karin R. Bryan[2], Mauricio E. Gonzalez[3], Antonio H.F. Klein[4], and Christian Winter[1]

Abstract

In order to decrease the simulation time of morphodynamic models, often-complex wave climates are reduced to a few representative wave conditions (RWC). When applied to embayed beaches, a test of whether a reduced wave climate is representative or not is to see whether it can recreate the observed equilibrium (long-term averaged) bathymetry of the bay. In this study, the wave climate experienced at Milagro Beach, Tarragona, Spain was discretized into 'average' and 'extreme' RWCs. The results of process-based, morphodynamic simulations were merged and used to estimate the equilibrium bathymetry of the bay, which were then compared to measurements. The most accurate outcome was obtained when at least 16 wave conditions were used. The effect of extreme wave events appeared to have less influence on the equilibrium of the bay, as indicated by improved results when average conditions were simulated. The importance of accounting for directional variability is essential to accurately balance the impact of beach rotation.

Key words: Equilibrium bathymetry, embayed beaches, representative wave conditions, input reduction, wave climate.

1. Introduction

The morphology of beaches is highly dependent on the local and regional wave climate as waves affect the beach orientation, beach slope, residual circulation pattern, and net sediment transport, both in the short- and long-term (Wright and Short, 1984; Short, 1996). The understanding of the variability and stability of sediment volumes on beaches is integral to sustainable coastal zone management and defense (Reeve and Li, 2009). This has led to much research interest in the long-term stability of beaches focusing on equilibrium concepts related to beach profiles (Bruun, 1954; Dean, 1990), and, with respect to embayed beaches, shoreline planforms (Yasso, 1965; Hsu and Evans, 1989; Moreno and Kraus, 1999). Open-coast beaches generally respond to wave forcing by shifting in the cross-shore direction, such as the on- and off-shore migration of sandbars (Pape and Ruessink, 2008). This holds true for embayed beaches; however, this usually results in beach rotation (Klein at al., 2002; Harley et al., 2011). Strong long-shore currents (and transport) may also develop within embayments when the incident wave direction is in disequilibrium with the existing bathymetry. These currents are reduced over time as the beach adjusts itself by rotating to form a more stable position (Daly et al., 2011). Alternating rotation events within an embayment may, over time, maintain some central tendency or equilibrium (LeBlond, 1979; Short and Masselink, 1999).

The combination of both equilibrium planform and profile formulae can be used to estimate the equilibrium bathymetry of an embayment (Hsu et al., 2010). However, this will tend to be over-simplified as the complexities of the geological setting and wave climate of the bay are largely ignored. For example, the equilibrium planform is usually determined based on a peak wave direction, therefore, the effect of other potentially morphologically-significant wave directions are ignored. In order to accurately determine the equilibrium bathymetry of an embayment, the variance of the wave climate and its influence on the net long-shore sediment transport (beach rotation events) should be taken into account. This can be done using process-based morphological models, which have proven to be useful tools in coastal research (e.g., Reniers et al., 2004; Castelle and Coco, 2012). However, as morphological simulations can be quite time consuming, it becomes necessary to reduce the wave climate to a number of representative wave conditions (hereafter *RWC*) (de Vriend et al., 1993; Plecha et al., 2007; Lesser, 2009).

[1]MARUM, University of Bremen, Leobener Strasse, 28000 Bremen, Germany. chrisdaly@uni-bremen.de
[2]Dept. Earth and Ocean Sciences, University of Waikato, Hamilton 3216, New Zealand.
[3]IH Cantabria, Avda de los Castros, 39005 Santander, Spain.
[4]Universidade Federal de Santa Catarina, Florianópolis, SC-88040-900, Brasil.

The wave climate in many parts of the world can be quite variable; some locations may have more than one dominant wave direction (bi-modal), while others may be frequently affected by random storm events. As such, it can be a challenge to reduce the wave climate to only a few RWCs while maintaining the important aspects of its variability. Accordingly, the performance of a reduced number of RWCs is best judged based on how well the morphology of the area of interest is reproduced. While there are several input reduction methods and approaches for applying or sequencing RWCs (e.g., Walstra et al., 2013; Benedet et al., submitted), there is still no standard method of doing so. Several uncertainties arise when trying to determine RWCs. For example, how many RWCs are necessary? What is the best way to discretize the wave climate? How do we account for storm conditions? Are storms important in the long run or do they get averaged out by more frequent, low-energy (average) conditions? What criteria should be used to determine weighting factors (frequency of occurrence, wave energy, sediment transport capacity, initial sedimentation-erosion (ISE) patterns)?

RWCs can be determined from the wave climate using one or two discretization stages, depending on the type of weighting factor used to scale the morphological influence of each RWC. The most common method to discretize the wave climate is to bin the data according to direction and wave height. When binned over a single stage, RWCs are determined directly from the data contained in each bin. This method is often used when determining weighting factors based on fixed wave height or wave energy bins; however, this approach ignores the non-linear relationship with sediment transport. Bulk sediment transport formulae (e.g., CERC, 1984) can be used as an indicator and are often casually applied to long, open coast beaches where waves have an uninterrupted approach the shoreline; however, this approach may lead to inaccurate representations of sediment transport when applied to embayed beaches as parts of the bay may be shadowed by headlands. The wave climate can also be discretized over two stages where, in the first stage, high resolution discrete wave conditions (hereafter *DWC*) are determined and then, in the second stage, reduced to a smaller number of RWCs (e.g., Mol, 2007). Weighting factors are then assigned to each DWC, usually based on the results of rapid morphodynamic simulations, where the initial sedimentation-erosion (ISE) pattern is computed, or hydrodynamic simulations, where the sediment transport potential related to a steady-state flow field is computed. When used as a proxy for weighting factors, the ISE associated to the DWCs are correlated to the net ISE, which is considered to be a target. DWCs whose ISE pattern is correlated to the target are preferably selected. Given that the net change in sediment volume and redistribution within an embayment can potentially be negligible over the long-term, the target ISE pattern will lie close to zero. Consequently, for embayed beach environments, the discrete ISE patterns will be largely uncorrelated to the target and therefore may not be suitable for determining weighting factors. The sediment transport potential is a more suitable parameter for determining weighting factors, as its total is non-zero and values can be assigned to each DWC.

In this study, we attempt to answer the questions raised above. In doing so, we use a two-step approach in which we first create DWCs and then group the DWCs into RWCs. We examine two methods to discretize the wave climate in order to determine DWCs by ranking the wave height, firstly, based on the frequency of occurrence and, secondly, based on the cumulative wave energy flux. A process-based morphological model is then used to estimate the equilibrium bathymetry of an embayed beach from RWCs by merging the results of several morphodynamic simulations. These results are then compared to observations of the beach bathymetry, and are followed by a brief summary and discussion of the findings.

2. Study Location and Available Data

The site chosen for the study is Milagro Beach in Tarragona, Catalonia, Spain (41.113°N, 1.258°E; Figure 1). The beach is approximately 1.2 km long and lies between a rocky headland outcrop to the north-west and a man-made marina to the south-east. The shoreline of the beach is curved, as is typical for embayments. The average beach width is approximately 35 m. The lengths of the headlands measured from the shoreline are approximately 120 m at the south-western headland and 200 m at the north-eastern headland. The maximum depths at the outer tip of the headlands (at the base) are approximately 6 m and 4.5 m respectively. This indicates that the beach slope at each headland is quite different, which is the result of an accumulation of sediment within the bay around the north-eastern headland. Sediment grain sizes vary from 0.125 mm around 15 m depth, 0.25 mm around 5 m depth, and 0.35 mm around the shoreline.

Figure 1 Bird's-eye view of Milagro Beach (image) in Tarragona, Catalonia, Spain (inset). Image from Google Maps

The beach experiences a wave climate typical for the north-west Mediterranean – a strong year-round occurrence of waves from the east and south, and energetic northerly storms during the winter (Garcia et al., 1993; Jiménez et al. 1997). Hourly hindcasted wave data is available for the area over a 44 year period between 1958 and 2001 (Ratsimandresey et al., 2008). Seven bathymetric surveys were undertaken over a 3.6 year period between February 1996 and October 1999. The bathymetric surveys were executed using a single beam echo sounder to measure depths along multiple cross-shore transects which extended out to approximately 20 m depth. Differences between surveys show that sediment was periodically redistributed within the bay, causing beach rotation as a result of changes in the peak wave direction over time. The observed tendency was for sediment to shift within the bay from the south-west to the north-east during winter months, and vice versa during summer months. All available bathymetric surveys of the study area were averaged in order to obtain an estimate of the expected equilibrium bathymetry, $z_{eq,meas}$ (Figure 2a).

3. Numerical Model Description and Setup

The open-source, process-based, numerical model, Delft3D (Lesser et al, 2004), was used to calculate the sediment transport potential of discretized wave conditions as well as to perform morphological simulations using RWCs as boundary conditions. Delft3D uses SWAN (Booij et al., 1999) to solve wave action balance equations. Radiation stresses calculated from SWAN are used to drive wave-induced flows in the nearshore. Non-cohesive sediment transport (bed load and suspended load) is computed according to van Rijn (1993). Morphodynamic updating is carried out at every time-step and can be accelerated using the 'Morfac' approach (Roelvink, 2006; Ranasinghe et al., 2011), whereby bed level changes computed over a single time-step are up-scaled by a morphological factor. The erosion of dry land is determined by associating a fraction of the erosion computed in an adjacent wet grid cell to the dry cell. The reader is directed to the Delft3D user manuals (http://oss.deltares.nl/web/delft3d/manuals) for detailed description of the numerical structure and formulations of the model.

A large wave grid (10 km × 20 km) was used to transform wave conditions from the deepwater boundary (100 m depth) towards the area of interest, where a smaller wave and flow grid (4 km × 4.5 km) was nested. The grid resolution in the area of interest was 20 × 20 m. Flow simulations were performed in a two-dimensional, depth-averaged (2DH) mode using a time step of 6 s. A 12 hour 'spin-up' period was used to establish hydrodynamic equilibrium before commencing morphological computations. A morphological acceleration factor of 12 was used and wave conditions were updated every 6 (morphological) hours. A median grain size of 0.25 mm was specified over the entire domain. The locations of impermeable, flow obstructing structures (headlands and breakwaters) were specified as dry cells (in the Delft3D flow module) and as obstacles (in SWAN). Hydrodynamic simulations (§4) used $z_{eq,meas}$ as the initial bathymetry. Morphodynamic simulations (§5) were initiated with an artificial bathymetry featuring a plane-sloped, arc-shaped beach between +1.5 and -3.5 m (Figure 2b) in order to reduce the bias of the simulation results toward $z_{eq,meas}$. The artificial initial bathymetry, z_{init}, maintains a similar volume of sediment in the bay as $z_{eq,meas}$.

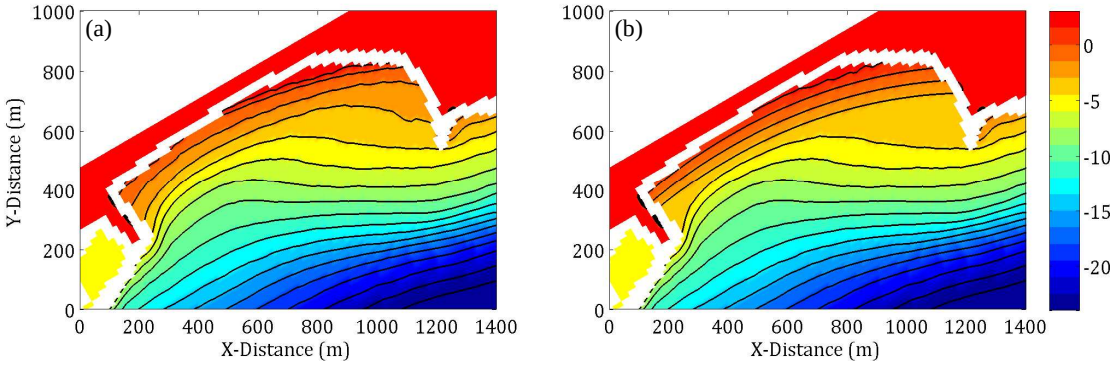

Figure 2 (a) Average of measured bathymetries of the bay, $z_{eq,meas}$. (b) Initial bathymetry used for morphodynamic simulations, z_{init}. Contours are drawn every 1.5 m between +1.5 m and -24 m

4. Method to Determine Representative Wave Conditions

The process of determining RWCs was done over two stages. In the first stage, the entire wave climate was divided into a number of discrete (high resolution) wave conditions (DWCs) and the sediment transport potential associated with each was determined from hydrodynamic simulations using Delft3D. The influence of each DWC on the morphology of the bay (i.e., weighting factor) was assumed to be the product of its sediment transport potential and frequency of occurrence. In the second stage, the high resolution DWCs were reduced to a number of (lower resolution) representative wave conditions (RWCs) by clustering the DWC weighting factors into equally distributed groups within a fixed number of directional bins. For both the DWCs and RWCs, each wave condition was defined by four variables, namely, significant wave height (H_s), peak period (T_p), direction (θ), and directional spreading (σ_θ).

4.1. *Stage 1: Determining Discrete Wave Conditions and Related Weighting Factors*

4.1.1. *Discrete Wave Conditions*

Four years of wave data were extracted from the available hindcast dataset between November 1995 and 1999 corresponding to the period during which bathymetric data were collected. Morphologically insignificant waves were removed from the data corresponding to observations in which the wave height was less than 0.5 m and in which the wave direction was greater than ± 120° of the primary heading of the beach (150° from the north). Those events represented 31% of the total wave climate. The remaining 69% of data were then divided into 24 wave directional *sectors* with a uniform width of 10°. Each sector was further divided into 10 equal *classes* by ranking the wave height based on the frequency of occurrence, P (hereafter *Method 1*), and by ranking the cumulative wave energy flux, E_f (hereafter *Method 2*), given as:

$$E_f = \frac{\rho g^2}{32\pi} H_s^2 T_p \tag{1}$$

where ρ is the density of water and g is gravitational acceleration. In the case of Method 1, the total number of observations within each class is constant within a sector. In the case of Method 2, the total amount of wave energy within each sector (i.e., the sum of E_f for all observations within each sector) was equally proportioned between each class (therefore, the top 90% – 100% class had less observations than the 0% – 10% class, and the value of P for the largest class was much smaller than for the smallest class). The 24 sectors and 10 classes yielded 240 discrete subdivisions of the wave climate (N_{dwc}), each referred to as a *cell*. Data associated within each cell were used to determine the DWC parameters. Wave heights associated with each DWC ($H_{s,dwc}$) were inversely determined from the average wave energy of the points within each cell, such that:

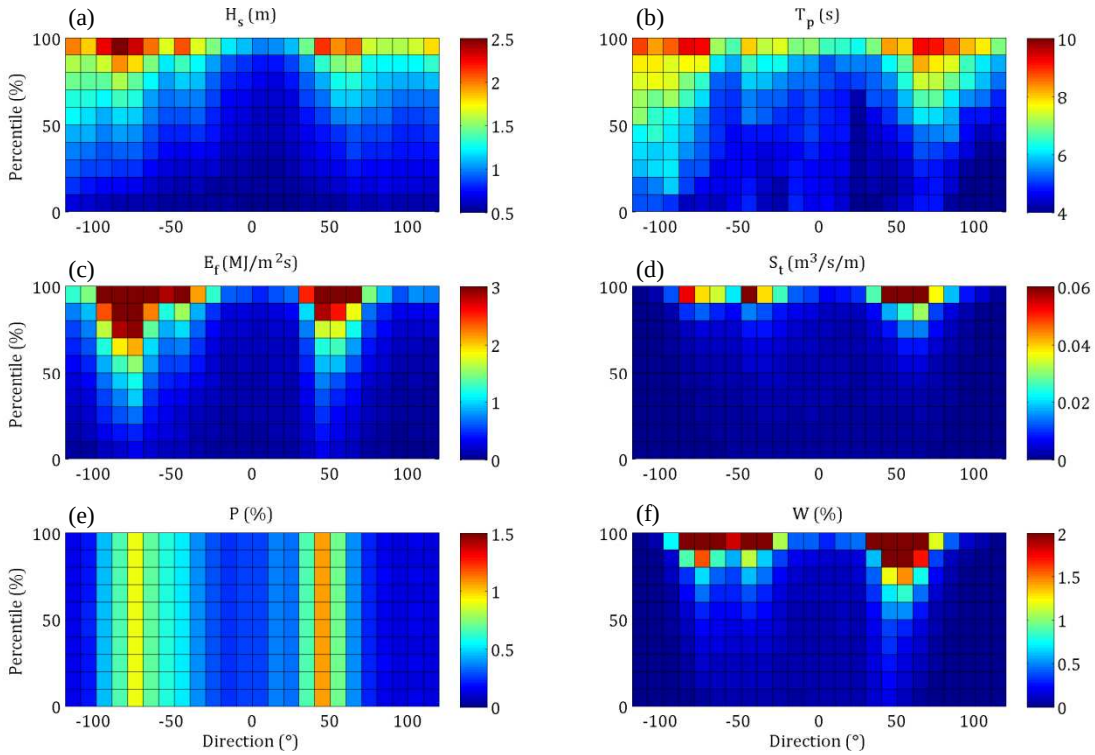

Figure 3 The discretized (high resolution) wave climate for Method 1. Within each cell is shown (a) H_s, (b) T_p, (c) E_f, (d) S_t, (e) P and (f) W. The color scale is indicated at the right of each plot and units shown in the title. The x- and y-axes are discretized in 24 directional sectors and 10 percentile classes of P, respectively

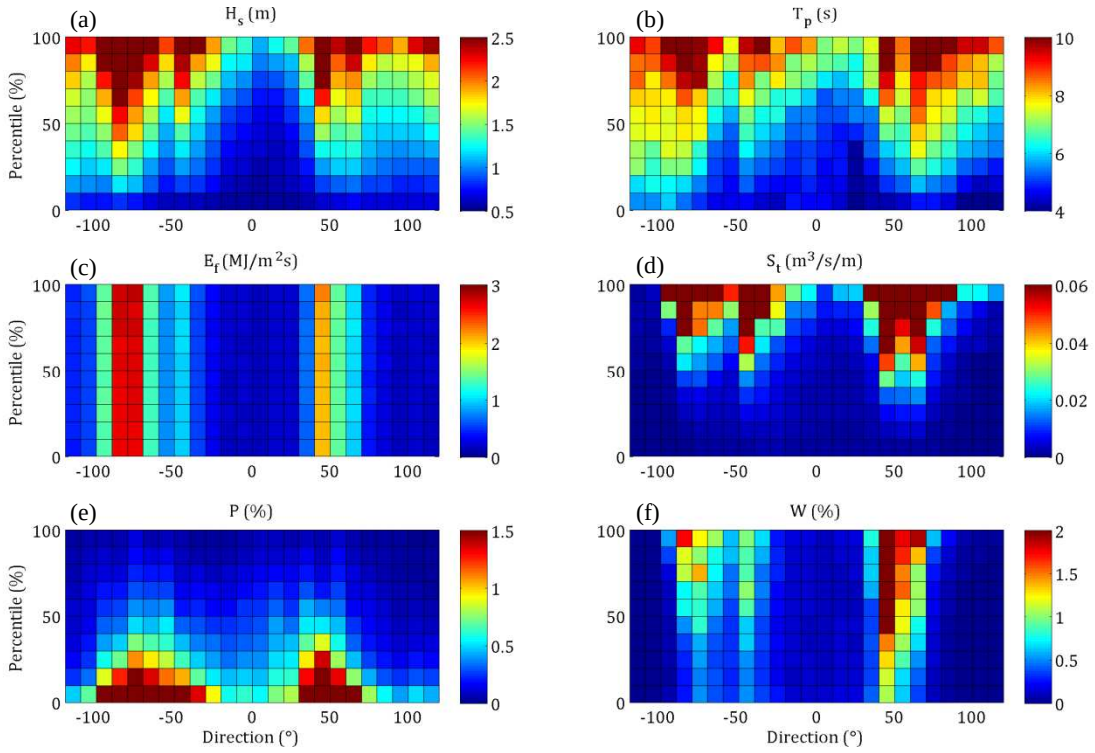

Figure 4 The discretized (high resolution) wave climate for Method 2. Within each cell is shown (a) H_s, (b) T_p, (c) E_f, (d) S_t, (e) P and (f) W. The color scale is indicated at the right of each plot and units shown in the title. The x- and y-axes are discretized in 24 directional sectors and 10 percentile classes of E_f, respectively

$$H_s = \sqrt{\frac{32\pi}{\rho g^2}\frac{\overline{E_f}}{\overline{T_p}}} \tag{2}$$

where the overbars represent averaging over the number of observations in each cell. Corresponding wave periods ($T_{p,dwc}$) within each cell were found by averaging the peak period associated with the data lying within a band $H_{s,dwc} \pm \sigma(H_{s,cell})$, where the subscript '*cell*' refers to the data points in each cell. The average and standard deviation of the wave directions within each cell is used as θ_{dwc} and $\sigma_{\theta,dwc}$, respectively.

4.1.2. *Discrete Weighting Factors*

The DWCs were used as the boundary conditions for a 2DH hydrodynamic simulation in order to determine the associated steady-state flow pattern. Each DWC was run for a 9-hour period without any morphological changes. The sediment transport induced by the steady-state flow pattern was then summed over the entire bay area and used to indicate how much sediment a particular DWC was capable of moving (i.e., the sediment transport potential, S_t). The sediment transport potential associated with each DWC was used as a proxy for the morphological significance of the event. Weighting factors associated with each DWC (W_{dwc}) were determined by multiplying its frequency of occurrence with its fraction of the total sediment transport potential, such that:

$$W_{dwc} = P_i \frac{S_{t,i}}{\sum_{i=1}^{N_{dwc}} S_{t,i}} \tag{3}$$

where the subscript '*i*' is used to index each DWC cell. The result of the discretization process is shown in Figure 3 and Figure 4 for Method 1 and Method 2, respectively. It is shown in these figures that Method 1 tends to give lower wave heights in each cell compared to Method 2 because lower wave heights are significantly more frequent than higher wave heights and higher wave heights possess significantly greater energy than lower wave heights. The sediment transport potential is, therefore, greater in magnitude for Method 2 than Method 1; however, the distribution is more-or-less similar, with peaks around the eastern and southern directions (-80° to -40° and 40° to 80°, respectively). Figure 5 shows the summed weighting factor as a function of wave direction and percentiles of P (for Method 1) and E_f (for Method 2). There, it is shown that the distribution of the weighting factor per wave direction is very similar for both methods; however, the distribution along the percentiles is different, with a more linear distribution given by Method 2 than Method 1. The sum of the weights within the 90th percentile for Method 1 accounts for 58% of the total weight, whereas for Method 2, the top 90th percentile accounts for only18%.

4.2. *Stage 2: Determining Representative Wave Conditions*

RWCs ($H_{s,rwc}$, $T_{p,rwc}$, θ_{rwc} and $\sigma_{\theta,rwc}$) were determined by, firstly, clustering the DWC cells into *groups* based on W_{dwc}. Groups were defined by binning the DWC cells into a smaller number of directions (N_θ). In this study, values of N_θ were 2, 4, 6, and 8. The total number of groups and, hence RWCs, (N_{rwc}) was equal to $2\times N_\theta$, thus, 4, 8, 12, and 16. The choice of the factor 2 was arbitrary and may be increased depending on the desired resolution of RWCs. The number of groups assigned to each directional bin ($N_{rwc,\theta}$) was equal to the (rounded) product of N_θ and the fraction of W_{dwc} present within each directional bin (W_θ) with a minimum of 1 RWC per directional bin.

If $N_{rwc,\theta}$ was greater than 1, then W_{dwc} was clustered into groups with approximately equal weight. The weight of each RWC, W_{rwc}, is simply the sum of the weight of the individual cells within each RWC group. In order to ensure an even distribution of W_{rwc} over $N_{rwc,\theta}$, its standard deviation was minimized by allowing discontinuities in a group (i.e. a group may consist of separated cells, as seen in Figure 6a). The maximum level of separation between cells in a group was limited to two cells.

RWCs were finally calculated in a similar manner as the DWCs with the exception that the reference to an individual cell was replaced by a reference to a group. Figure 6 and Figure 7 show the result of the clustering process and also the values of $H_{s,rwc}$ and θ_{rwc}. It should be noted that values of $H_{s,rwc}$ obtained using Method 2 are significantly higher than those obtained using Method 1. Method 1, therefore, yields RWCs that are comparable to average conditions, while Method 2 is biased toward extreme events.

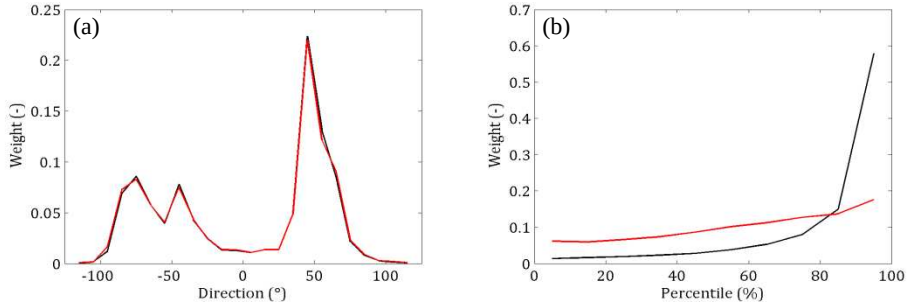

Figure 5 Weighting factor, W_{dwc}, plotted over the (a) wave direction and (b) percentiles of P (for Method 1, black line) and percentiles of E_f (for Method 2, red line)

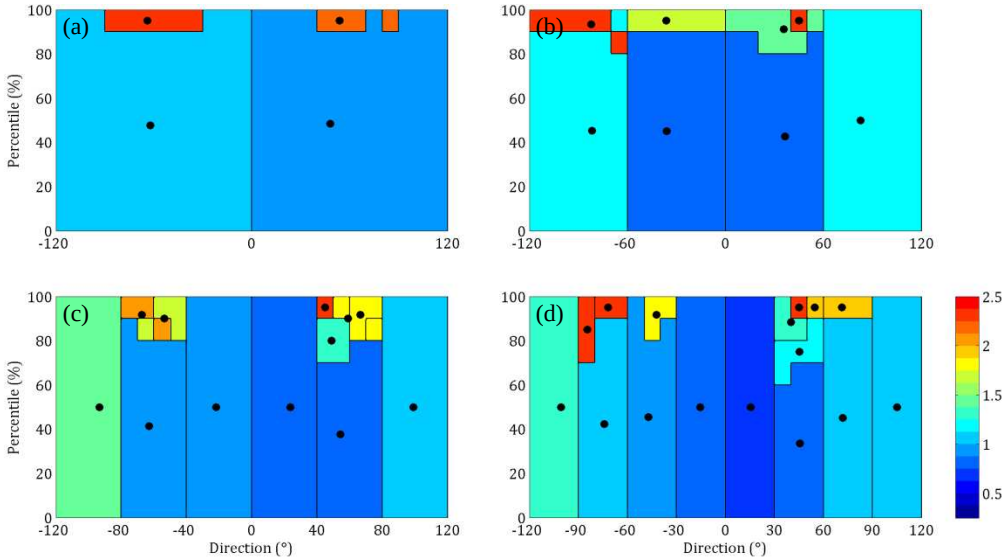

Figure 6 Clustering of RWC bins for (a) 4 bins, (b) 8 bins, (c) 12 bins, and (c) 16 bins for Method 1. The color scale and the position of the black dots relative to the x-axis indicates the value of $H_{s,rwc}$ and θ_{rwc}, respectively

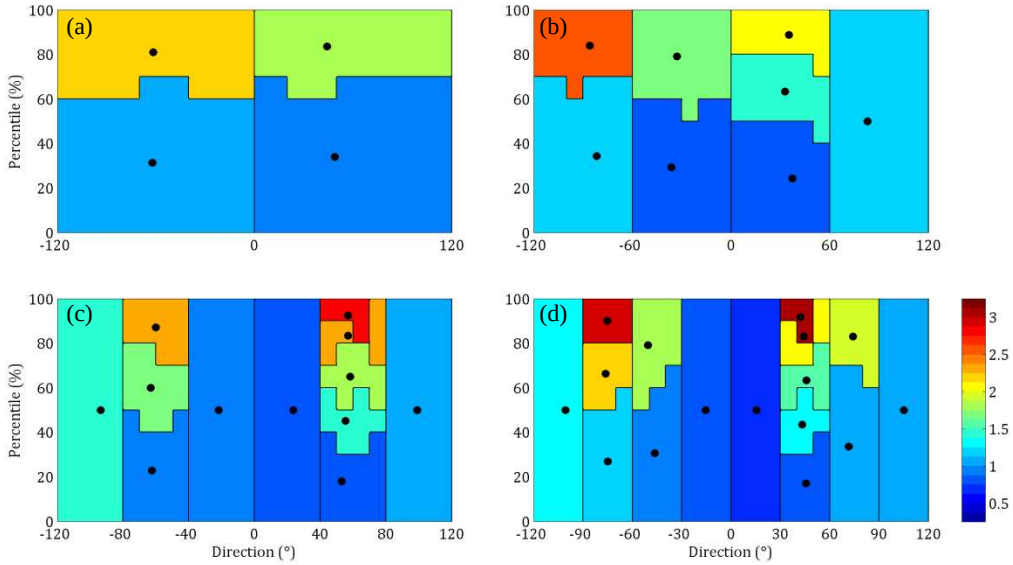

Figure 7 Clustering of RWC bins for (a) 4 bins, (b) 8 bins, (c) 12 bins, and (c) 16 bins for Method 2. The color scale and the position of the black dots relative to the x-axis indicates the value of $H_{s,rwc}$ and θ_{rwc}, respectively

5. Morphodynamic Simulation Results

After RWCs were determined, they were each used as the boundary condition for morphological simulations. The wave forcing was kept constant during each simulation and the duration of each simulation (D_{rwc}) was equal to the product of the weighting factor of a particular RWC (W_{rwc}) and the total period under consideration (D), which is equal to 4 years, such that:

$$D_{rwc} = D \cdot W_{rwc} \tag{4}$$

D_{rwc} is therefore equivalent to the morphological duration of each RWC. The final bathymetry from each simulation was averaged to obtain an estimate of the equilibrium bathymetry of the bay, $z_{eq,rwc}$, given as:

$$z_{rwc} = \frac{1}{N_{rwc}} \sum_{j=1}^{N_{rwc}} z_j \tag{5}$$

where the subscript '*j*' is used to index each RWC. The morphological simulations of RWCs are not run sequentially as this is typically done to mimic a time-series of wave conditions. As we are interested in the time-averaged bathymetry, then the average outcome of the morphological simulations of RWCs should resolve the rotation pattern of the beach.

Figure 8 and Figure 9 show the raw difference between the observed and predicted equilibrium bathymetries. The comparison between $z_{eq,rwc}$ and $z_{eq,meas}$ improves as N_{rwc} increases. In all cases, $z_{eq,rwc}$ was over-predicted in the north-east section of the beach (accretion) and under-predicted in the south-west section of the beach and between 4.5 – 9 m depth (erosion). This caused $z_{eq,rwc}$ to appear to be rotated by 5 – 10° when compared to $z_{eq,meas}$. In all cases, the upper section of the beach between 0 – 3 m appeared to be reconstructed fairly well given the difference between z_{init} and $z_{eq,\,meas}$. This is best seen by noting the shape of the 3 m contour line for $z_{eq,rwc}$ and $z_{eq,\,meas}$. In order to strictly assess the performance of the models and, hence, the validity of the different methods of determining the RWCs, the Brier Skill Score (BSS) and root-mean-square error (RMSE) was calculated for each simulation, given as:

$$BSS = 1 - \frac{\sum \overline{(|\, z_{eq,rwc} - z_{eq,meas} \,| - \varepsilon_{meas})}^2}{\sum \overline{(z_{init} - z_{eq,meas})}^2} \tag{6}$$

$$RMSE = \sqrt{\overline{(z_{eq,rwc} - z_{eq,meas})}^2} \tag{7}$$

where ε_{meas} is the measurement error, assumed to be in the order of 0.1 m. BSS values less than 0 indicate a *bad* result (the initial condition was better than the final result), while values between 0 – 0.3, 0.3 – 0.6, 0.6 – 0.8 and 0.8 – 1 are classed *poor*, *reasonable*, *good*, and *excellent*, respectively (van Rijn et al., 2003). Table 1 shows the BSS and RMSE for each simulation, where it is shown that Method 1 produced better results than Method 2. According to the classification, bad results were obtained for cases with N_{rwc} = 4, and poor results for all other cases with the exception of N_{rwc} = 16 for Method 1, which had a reasonable result.

Table 1. Model performance (RMSE and BSS)

N_{rwc}	Method 1		Method 2	
	RMSE (m)	BSS (–)	RMSE (m)	BSS (–)
4	0.32	-0.35	0.35	-0.63
8	0.24	0.23	0.26	0.11
12	0.23	0.29	0.26	0.05
16	0.22	0.37	0.24	0.21

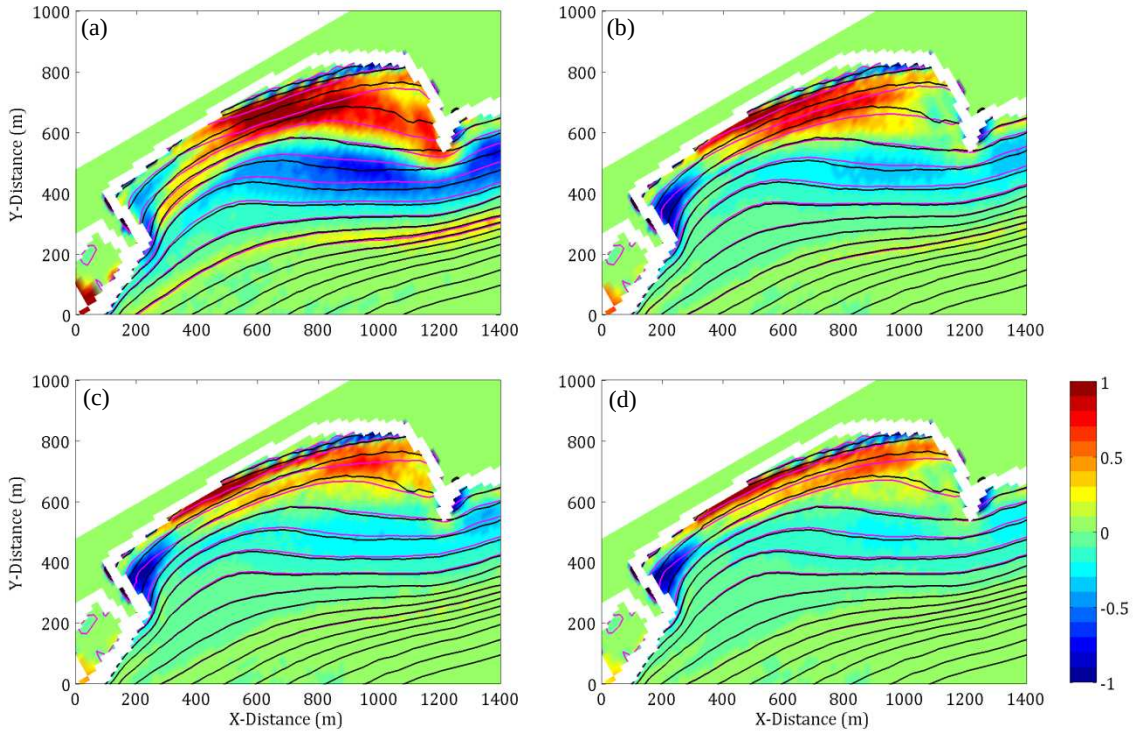

Figure 8 Difference (color scale) between $z_{eq,meas}$ (black contours) and $z_{eq,rwc}$ (pink contours) where N_{rwc} = (a) 4, (b) 8, (c) 12, and (d) 16, for Method 1. Contours are drawn every 1.5 m between +1.5 m and -24 m

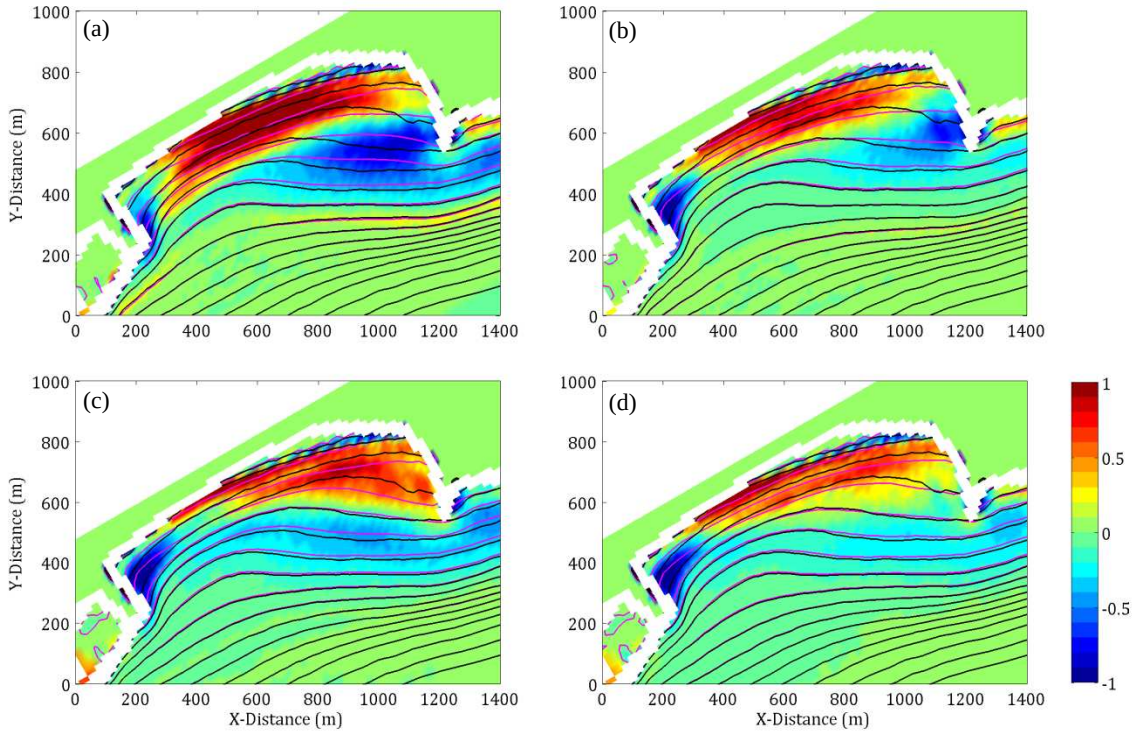

Figure 9 Difference (color scale) between $z_{eq,meas}$ (black contours) and $z_{eq,rwc}$ (pink contours) where N_{rwc} = (a) 4, (b) 8, (c) 12, and (d) 16, for Method 2. Contours are drawn every 1.5 m between +1.5 m and -24 m

6. Discussion

Two methods of determining DWCs have been shown and used to determine RWCs, which were then used to simulate the equilibrium bathymetry of an embayment. Discretizing the wave climate by binning the wave height according to the frequency of occurrence (Method 1) yields RWCs that are analogous to 'average' forcing conditions, whereas binning according to the wave energy (Method 2) shifts the RWCs toward more 'extreme' forcing conditions. As Method 1 resulted in better simulation results, we can infer that the role of extreme conditions is less significant than the average conditions. This would suggest that the magnitude of morphological changes caused by extreme events is adequately balanced by calmer events of significantly longer duration. It was also shown that by increasing the number of RWCs the effect of beach rotation and sediment accumulation at both ends of the beach and within the foreshore was better resolved. This suggests that increased directional resolution is important in determining the right balance for wave directions, which can potentially cause strong beach rotation events. Linear increases in N_{rwc} resulted in a non-linear improvement of model results (i.e., reduced RMSE and increased BSS). By extrapolation, a minimum of 16 – 20 wave conditions are necessary to adequately account for the observed morphological equilibrium, a similar finding of Walstra et al. (2013).

The BSS for most of the simulations indicate less than desirable results when $z_{eq,rwc}$ is compared to $z_{eq,meas}$, which could be due to several reasons: (1) measurement error, (2) model error, and (3) application of the proposed input reduction method. In the case of (1), the number of observations used to determine $z_{eq,meas}$ was quite low; only seven measurements over a four-year period. A better estimate could be attained if at least quarterly surveys were done, capturing more of the annual variance of bed levels in the bay. In the case of (2), model results may be improved by including additional processes (e.g., undertow or diffraction) or by performing a more robust calibration of model parameter settings. In the case of (3), more highly resolved DWCs would permit more optimal clustering of RWCs. For example, doubling the resolution of DWCs used in this study would allow the upper 10% of data to be better clustered into groups when applying Method 1. Additionally, a greater number of wave directional bins could be used for the RWCs. In this study, the smallest bin size was 30°; however, a 15° bin size may increase the accuracy of the results by accounting for a greater number of wave directions. Lastly, it was shown that waves greater than ± 100° of the shore normal have a very weak influence on the morphology of the bay, therefore, these conditions may be ignored in order to improve the assignment of RWCs.

Despite the abovementioned limitations, the results obtained from this study support the proposition that an equilibrium state exists for embayed beaches, which is largely controlled by the wave climate, and in particular, the wave direction. This equilibrium state may be transient if the long-term wave climate gradually changes over time. It should be noted that single observations of the embayment bathymetry may be significantly different from the equilibrium case depending on the short-term wave conditions (Reeve and Li, 2009). However, the proposed input reduction method can be used to provide information on the expected maxima and minima (and, hence, expected variance) of bed levels within embayed beach environments, which may be useful for coastal zone management and defense strategies.

7. Conclusion

The equilibrium bathymetry of an embayed beach was determined using a varied number of RWCs. Two methods of calculating the weight assigned to the RWCs were also compared. Results indicate that binning wave heights in terms of frequency of occurrence gives better results than binning according to wave energy. A minimum of 16 RWCs produced reasonably skillful results despite using rather standard model settings. Given that there is enough room for improvement, the present results are promising and indicate that the equilibrium bathymetry within embayments is largely determined by a variable wave climate, especially in relation to the wave direction. It is therefore necessary to ensure that a suitable level of directional resolution is accounted for when determining RWCs for embayed beach environments.

Acknowledgements

C.J. Daly acknowledges research funding from the German Research Foundation (DFG) via the International Research Training Group: Integrated Coastal Zone and Shelf Sea Research (INTERCOAST). The field data has been kindly provided by Dr. Jordi Galofré (Spanish Ministry of Environment), and its support is hereby gratefully acknowledged.

References

Benedet, L., Dobrochinski, J., Ranasinghe, R., Klein, A. and Walstra, D.J.R., submitted. Wave climate schematization for morphological modeling of open ocean beaches: analysis of methods and application to the Delray Beach case study, *Journal of Coastal Engineering*.

Booij, N., Ris, R.C. and Hotlhuijsen, L.C., 1999. A third-generation wave generation model for coastal regions, Part I: Model description and validation, *Journal of Geophysical Research*, 104: 7649–7666.

Bruun, P., 1954. *Coastal erosion and the development of beach profiles*, Technical Memorandum No. 44, US Army Corps of Engineers, Beach Erosion Board, Washington D.C.

Castelle, B. and Coco, G., 2012. The morphodynamics of rip channels on embayed beaches, *Journal of Continental Shelf Research*, 43: 10–23.

CERC (Coastal Engineering Research Center), 1984. *Shore Protection Manual*, US Army Corps of Engineers, Waterways Experiment Station, Washington D.C.

Daly, C.J., Bryan, K.R., Roelvink, J.A., Klein, A.H.F., Hebbeln, D. and Winter, C., 2011. Morphodynamics of embayed beaches: The role of wave conditions, *Journal of Coastal Research*, SI 64: 1003–1007.

Dean, R.G., 1990. *Equilibrium Beach Profiles: Characteristics and Applications*, Department of Coastal Engineering, University of Florida, Gainesville.

de Vriend, H., Capobianco, M., Chesher, T., de Swart, H.E., Latteux, B. and Stive, M.J.F., 1993. Approaches to long term modeling of coastal morphology: A review, *Journal of Coastal Engineering*, 21: 225–269.

Garcia, M.A., Sánchez-Arcilla, A., Sierra, J.P., Sospedra, J. and Gómez, J., 1993. Wind waves off the Ebro Delta, NW Mediterranean, *Journal of Marine Systems*, 4(2/3): 235–262.

Harley, M.D., Turner, I.L., Short, A.D. and Ranasinghe, R., 2011. A reevaluation of coastal embayment rotation: The dominance of cross-shore versus alongshore sediment transport processes, Collaroy-Narrabeen Beach, southeast Australia, *Journal of Geophysical Research*, 116, F04033, doi:10.1029/2011JF001989.

Hsu, J.R.C., Yu, M.J., Lee, F.C. and Benedet, L., 2010. Static bay beach concepts for scientists and engineers: A review, *Journal of Coastal Engineering*, 57: 76–91.

Hsu, J.R.C. and Evans, C., 1989. Parabolic bay shapes and applications, *Proceedings of the Institute of Civil Engineers*, 87: 557–570.

Jiménez, J.A., Sánchez-Arcilla, A., Valdemoro, H.I., Gracia, V. and Nieto, F., 1997. Processes reshaping the Ebro Delta, *Journal of Marine Geology*, 144: 59–79.

Klein, A.H.F., Benedet, L.F. and Delamar, H.S., 2002. Short-term beach rotation processes in distinct headland bay beach systems, *Journal of Coastal Research*, 18(3): 442–458.

LeBlond, P.H., 1979. An explanation of the logarithmic spiral plan shape of headland-bay beaches, *Journal of Sedimentary Petrology*, 49(4): 1093–1100.

Lesser, G.R., 2009. *An approach to medium-term coastal morphological modeling*. Ph.D. Thesis, Delft University of Technology, CRC Press/Balkema, ISBN 978-0-415-55668-2.

Lesser, G.R., Roelvink, J.A., van Kester, J.A.T.M. and Stelling, G.S., 2004. Development and validation of a three-dimensional morphological model, *Journal of Coastal Engineering*, 51: 883–915.

Mol, A.C.S., 2007. *Schematization of boundary conditions for morphological simulations*. Research report, WL | Delft Hydraulics, The Netherlands.

Moreno, L.J. and Kraus, N.C., 1999. Equilibrium shape of headland-bay beaches for engineering design, *Proceedings 4th International Symposium on Coastal Sediments*, American Society of Civil Engineers, pp. 860–875.

Pape, L. and Ruessink, B. G., 2008. Multivariate analysis of nonlinearity in sandbar behavior, *Nonlinear Processes in Geophysics*, 15: 145– 58.

Plecha, S., Sancho, F., Silva, P. and Dias, J.M., 2007. Representative waves for morphological simulations, *Journal of Coastal Research*, SI 50: 995–999.

Ranasinghe, R., Swinkels, C., Luijendijk, A., Roelvink, J.A., Bosboom, J., Stive, M.J.F. and Walstra, D.J.R., 2011. Morphodynamic upscaling with the MorFac approach: dependencies and sensitivities, *Journal of Coastal Engineering*, 58: 806–811.

Ratsimandresy, A.W., Sotillo, M.G., Carretero Albiach, J.C., Álvarez Fanjul, E. and Hajji, H., 2008. A 44-year high-resolution ocean and atmospheric hindcast for the Mediterranean Basin developed within the HIPOCAS Project, *Journal of Coastal Engineering*, 55: 827–842.

Reeve, D.E. and Li, Y., 2009. Stochastic model for embayed beaches, *Journal of Waterway, Port, Coastal and Ocean Engineering*, American Society of Civil Engineers, 144–153.

Reniers, A.J.H.M., Roelvink, J.A. and Thornton, E.B., 2004. Morphodynamic modelling of an embayed beach under wave group forcing, *Journal of Geophysical Research*, 109, C01030, doi:10.1029/2002JC001586

Roelvink, J.A., 2006. Coastal morphodynamic evolution techniques, *Journal of Coastal Engineering*, 53, 277–287.

Short, A.D., 1996. The role of wave height, period, slope, tide range and embaymentisation in beach classifications: A review, *Journal Revista Chilena de Historia Natural*, 69: 589–604.

Short, A.D. and Masselink, G., 1999. Embayed and Structurally controlled beaches in: *Handbook of Beach and Shoreface Morphodynamics*, pp 230-249.

van Rijn, L.C., 1993. *Principles of Sediment Transport in Rivers, Estuaries and Coastal Seas*. Aqua Publications, The Netherlands.

van Rijn, L.C., Walstra, D.J.R., Grasmeijer, B., Sutherland, J., Pan, S. and Sierra, J.P., 2003. The predictability of cross-shore bed evolution of sandy beaches at the time scale of storms and seasons using process-based profile models, *Journal of Coastal Engineering*, 47: 295–327.

Walstra, D.J.R, Hoekstra, R., Tonnon, P.K. and Ruessink, B.G., 2013. Input reduction for long-term morphodynamic simulations in wave-dominated coastal settings, *Journal of Coastal Engineering*, 77: 57–70.

Wright, L.D. and Short, H.D., 1984. Morphodynamic variability of surf zones and beaches: A synthesis, *Journal of Marine Geology*, 56: 93–118.

Yasso, W.E., 1965. Plan geometry of headland bay beaches, *Journal of Geology*, 73: 702–714.